AIChE

Low-Temperature Conversion of Spent Adsorbent to Iodine Sodalite by a Mechanochemical Route

D. Hirabayashi, Y. Tanada, T. Sugiyama, and Y. Enokida
Dept. of Materials, Physics and Energy Engineering, Graduate School of Engineering, Nagoya University, Nagoya, 464-8603, Japan

K. Sawada
EcoTopia Science Institute, Nagoya University, Nagoya, 464-8603, Japan

DOI 10.1002/aic.12756
Published online October 11, 2011 in Wiley Online Library (wileyonlinelibrary.com).

The focus on a ball milling induced conversion as a possible synthesis route of iodine sodalite ($Na_8Al_6Si_6O_{24}I_2$) from zeolite-based iodine adsorbents in order to treat a radioactive iodine filter for the off-gas cleaning during nuclear facilities is presented. A mixture of silver iodide and zeolite 13X as a simulated adsorbent was mechanochemically milled using a laboratory-scale planetary ball mill. The obtained powders were characterized by X-ray diffraction to determine the effect of milling time on the conversion of the iodine sodalite. The crystal grain size and the lattice strain of the grounded phases were evaluated. After the ball milling, the milled samples were hydrothermally crystallized to form a sodalite phase with a sodium hydroxide solution for 48 h in an autoclave maintained at 150°C. The iodine sodalite was successfully obtained after hydrothermal crystallization. A leaching test was carried out for the assessment of the order of iodine leachability and chemical durability under reducing conditions. The leaching amount was found to be low on the orders of 10^{-4} ~10^{-5} mol dm^{-3} in sodium thiosulfate solution. © 2011 American Institute of Chemical Engineers *AIChE J,* 58: 2441–2447, 2012
Keywords: radioactive iodine, spent adsorbent, iodine sodalite, mechanochemical conversion, immobilization

Introduction

Iodine-129 is a radioactive form of iodine as a product of nuclear fission of heavy nuclides such as uranium-235. Iodine nuclides are present in the high-level radioactive wastes resulting from processing spent nuclear fuel and the radioactive wastes associated with the operation of nuclear reactors. During the reprocessing processes, iodine-129 is transferred from the liquid phase to the vapor phase, where iodine-129 is trapped in a silver-containing adsorbent, such as silver zeolite,[1,2] as a form of silver iodide AgI, from the off-gas stream.[3] However, silver iodide is unstable under the reducing conditions in a geological repository[4] and iodine-129 has a long half-life of about 15.7×10^6 years, and, therefore, it becomes a significant long-term source of radioactivity. Moreover, because iodine dissolves as an anionic form easily and moves down with percolating water to the groundwater, the long-term immobilization of iodine-129 is one of the great concerns to researchers for the geological disposal of radioactive waste containing transuranic elements.

To immobilize radioactive iodine, several matrices have been investigated.[5–8] Among them, iodine sodalite, $Na_8Al_6Si_6O_{24}I_2$, is considered as one of the insoluble crystalline forms candidates.[9–12] Sodalite is a type of zeolite, a natural and artificially synthesized mineral, which includes several anionic species and groups (OH^-, Cl^-, Br^-, I^-, etc.),[12] and alkaline metal cations (Li^+, K^+, Na^+, Cs^+, etc.).[14] The solubility of sodalite (10^{-5} mol dm^{-3}) is independent of the environmental atmosphere due to its high tolerance to a reducing atmosphere in some deep underground storage facilities. The sodalite phase has a framework of cubic symmetry with a strictly alternating connection of corner sharing SiO_4 and AlO_4 tetrahedra. The framework of the sodalite cages is highly flexible and can accommodate a certain degree of expansion due to guest species of different sizes. According to the literature,[15] one possible synthesis procedure of iodide sodalite from AgI-containing zeolite was a solid-state conversion at a high temperature in an electric oven. In this route, iodine sodalite can be obtained above 800°C. This is because the ionic radius of iodide ions (0.22 nm) was relatively large compared to the open-pore radius of the sodalite cage (0.28 nm) without thermal expansion. However, excessive heating at higher temperatures enhances the thermal decomposition and volatilization of silver iodide over the melting temperature, resulting in the serious emission of radioactive iodine.

This study presents a new and novel procedure for the conversion of the zeolite-based iodine adsorbents to iodine sodalite by a mechanochemical method instead of the conventional thermal conversion. The schematic of a ball milling process is shown in Figure 1. It was theorized that if the mechanochemical conversion by ball milling was used instead of a thermal treatment, a precursor of iodine sodalite, which was activated and strained with some formation of

Correspondence concerning this article should be addressed to D. Hirabayashi at hirabayashi@nagoya-u.jp.

© 2011 American Institute of Chemical Engineers

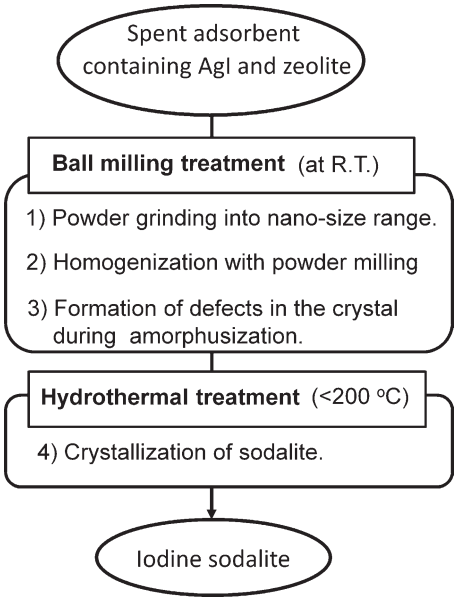

Figure 1. Schematics of a ball milling process from a spent adsorbent to iodine sodalite by a mechanochemical route.

defects in the crystal structure by grinding in a nanoscale size range, would be produced at low temperature. Furthermore, we considered that, if the uniform fine mixture of zeolite and silver iodide was obtained by ball milling, an extra step, the thermal treatment for mass transfer would not be required. In the experiment, the crystalline phases included in the final product were characterized using an X-ray diffractometer to confirm the effect of milling time. The lattice parameters, crystalline sizes and lattice strains were estimated from the diffraction profiles of faujasite, sodalite and silver iodide phase. The leachability of iodine was also studied using the MCC-3 standard leach method. The leaching amount of iodine for 14 days was measured in ultrapure water and a sodium thiosulfate solution as the leachant.

Experimental

A mixture of silver iodide and zeolite 13X as the simulated adsorbent of a spent iodine filter was milled using the planetary ball mill with different milling times of 3, 6, 12, 24 and 48 h. The starting chemicals of AgI (>99.9% in purity), and zeolite 13X (molecular sieve 13X, $1\frac{1}{6}$ in. in diameter, pellet shape) were purchased from Wako Pure Chemical Industries, Ltd. The zeolite 13X pellets as received were dried at 150°C in an oven.

In a typical experimental procedure, the mixture of silver iodide and zeolite 13X were ground into powders in an agate mortar. The amount of silver iodide was initially chosen such that the mass ratio of silver iodide to zeolite 13X was 1:10. The milling equipment consisted of a planetary ball mill (Frisch, Pulverisette P-7, Germany) with tungsten carbide vials, whose inner volume is 0.025 dm^{-3}, and tungsten carbide balls. A sample-to-ball weight ratio of 1:30 was used in the milling operations. Grinding of the powders was carried out in air at a rotation speed of 700 rpm. The operation did not cause a significant increase of the temperature. The temperature just after the grinding heat and ranged from 30 to 40°C at 700 rpm depending on the grinding time and batch. Sodium hydroxide solutions (6 mol dm^{-3}) were used for activation of the hydrothermal reaction[16] during the sodalite crystallization. After the ball milling, a gray powder was formed, and then the powder was poured into a polytetrafluoroethylene (PTFE) vessel of 0.040 dm^{-3} in volume. The vessel was placed in a stainless autoclave with 0.2 g of sodium hydroxide solution in the bottom. The crystallization of the milled powder was carried out at 150°C for 48 h under autogenous pressure.

After the crystallization completed, the autoclave was quenched in static air, and the sample was removed from the PTFE vessel, washed with distilled water and dried around 100°C. The powder X-ray diffraction was measured by an XRD diffractometer (mini-flex, RIGAKU, Japan) with Cu Kα radiation (λ = 0.1542 nm, 30 kV, 15 mA). Scanning electron micrograph images were observed using a scanning electron microscope (SEM, JSM-6390AH, JEOL, Japan) at 10 kV. The diffraction pattern were obtained in the range of 2θ = 20–80° at a step of 0.01°. The X-ray diffraction of the different milling times was performed for the milled samples and their hydrothermal products at the different milling stages. The elemental distribution of the crystal surfaces was investigated by SEM-EDS for the elements of Na, Si, Al, Ag and I.

The MCC-3 leaching test method[17] was used for the assessment of the order of iodine leachability. An experimental setup for the leachability test is displayed in Figure 2. The obtained samples after hydrothermal treatment were crushed in a mortar and sieved to 63–100 μm. The samples were placed in 0.04 dm^{-3} PTFE vessels containing ultrapure water for the oxidizing condition or 0.1 mol dm^{-3} sodium thiosulfate solutions for reducing condition. All handling of materials for the test under reducing conditions was carried out in a glovebox under a controlled argon atmosphere to

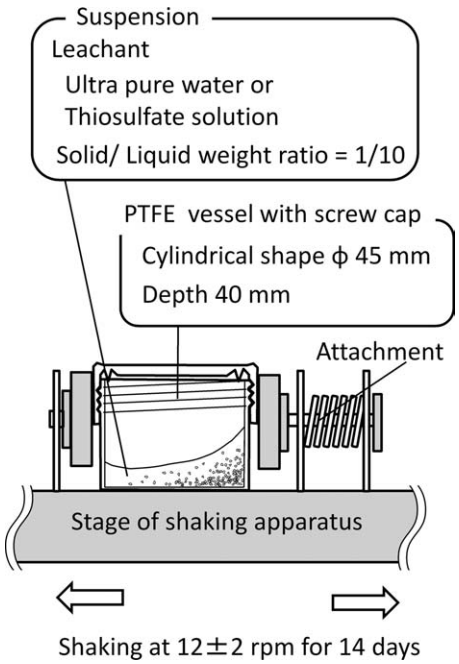

Figure 2. Experimental setup of the leachability test in accordance with MCC-3 method.

PTFE vessels containing test suspensions were fixed by attachments on a stage of shaking apparatus.

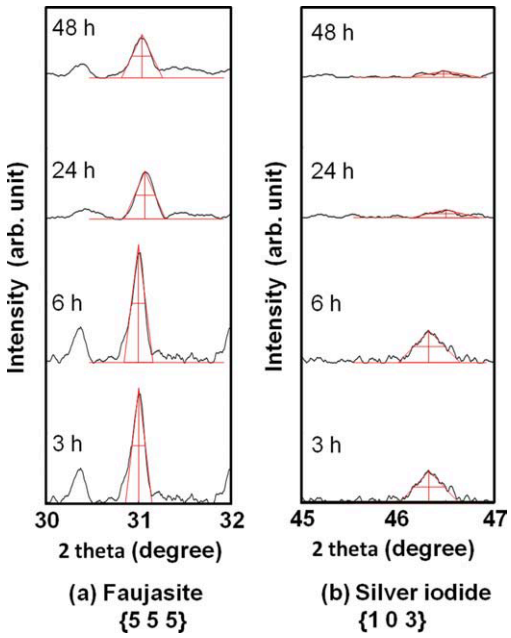

Figure 3. Close up view of diffraction profiles around the diffraction peaks; (a) {5 5 5} for faujasite, (b) {1 0 3} for AgI.

[Color figure can be viewed in the online issue, which is available at wileyonlinelibrary.com.]

avoid oxygen contamination of the vessel. The gap between the vessel and cap was tightly sealed with PTFE tape. The weight ratio of the sample to the leachant was maintained at a constant of 1:10. The test was carried out at room temperature for 14 days followed by the quantitative analysis of iodine using induction coupled plasma mass spectrometry (ICP-MS, SPQ-9700, Bruker, Australia).

Results and Discussion

Effects of ball milling on crystal parameters of raw mixture

Based on the XRD, the crystal phase of the as-received zeolite 13X was determined as sodium faujasite 13X, $Na_2Al_2Si_4O_{12}.8H_2O$ and the silver iodide was γ-AgI. Figure 3 shows a close up of diffraction profiles around the diffraction peaks; (a) {5 5 5} for faujasite, and (b) {1 0 3} for silver iodide. After ball milling, the diffraction peaks of both phases tended to be broaden as the milling time increased. Both phases were clearly present in the starting material, but the silver iodide phase was absent after 24 h or longer milling.

The crystal grain size D, and the lattice strain ϵ, were evaluated for each phase in order to investigate the broadening effects of the diffraction peaks by ball milling. The crystal grain size was calculated from the peak width of the intense peak using the Scherrer's equation[18]

$$D = \frac{0.89\lambda}{\beta_{1/2}\cos\theta} \tag{1}$$

where $\beta_{1/2}$ is the half peak width and λ is the wavelength of the X-ray radiation. The value of $\beta_{1/2}$ was determined from the experimental integral peak width (FWHM). The crystal grain size evaluated from peak width is plotted in Figure 4. The crystal grain sizes of faujasite remarkably decreased from 370 to 90 nm with an increase in the milling time and reached saturation values over 24 h. Likewise, the crystal grain size of silver iodide gradually decreased from 60 to 40 nm, although the decrease was much lower than that of faujasite. This suggests that both phases tended to be either amorphous or consist of extremely small, highly disordered crystals at the final stage of ball milling, and the ball milling more strongly affected the grinding of the faujasite particles and its crystal grains.

The lattice strain on the lattice plane was estimated from the ratio of the variation in the crystal face accounting for the nonstrain state by applying following equation

$$\varepsilon = \frac{\Delta d}{d_0} = \frac{d - d_0}{d_0} \tag{2}$$

The lattice strain for evaluated each phase was plotted versus ball milling time as shown in Figure 5. Strain in the faujasite phase varied around 0.002 from the beginning of milling to 12 h, however, the strain rapidly increased to 0.026 at 24 h. On the other hand, change in the strain of the silver iodide phase remained low around + 0.0002–0.0003 even after a long milling time. These results indicated that a part of the mechanical energy is used in breaking the faujasite particles, and another part is used in creating the defects, such as dislocations, and the distortion of the lattice in faujasite. In other words, the mechanical energy provided by ball

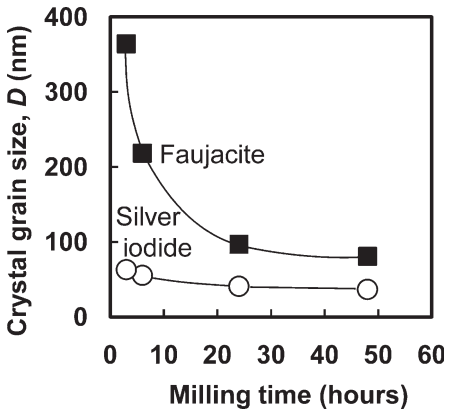

Figure 4. Effect of milling time on crystal grain size, *D* of faujasite (squares) and AgI (circles) crystals.

The crystal grain size was estimated from the intense peaks {5 5 5} for faujasite and at {1 0 3} for AgI.

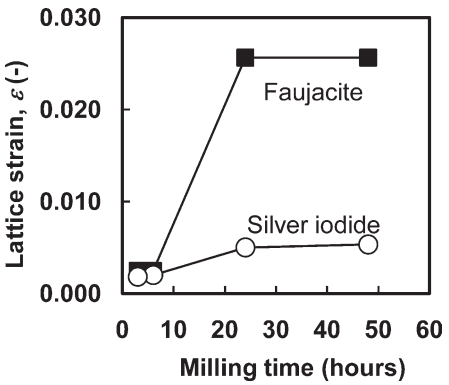

Figure 5. Effect of milling time on lattice strain, ϵ of faujasite {5 5 5} (squares) and γ-AgI crystals {1 0 3} (circles).

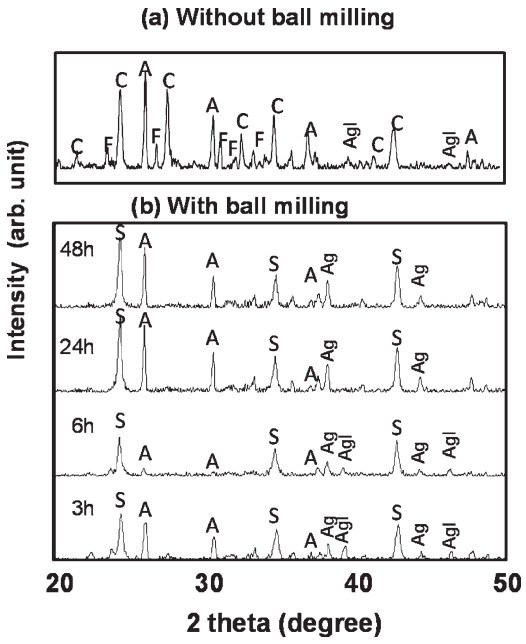

C	hydroxyl cancrinite JCPDS 31-1272
F*	Faujasite-Na, syn JCPDS 39-1380
A	Analcime-O JCPDS 19-1180
AgI*	γ-type silver iodide JCPDS 09-0399
S	Iodine sodalite JCPDS 81-0107
Ag	Metallic silver JCPDS 04-0783

* Initial phases detected in the mixture before ball milling.

Figure 6. XRD results of obtained powders after hydrothermal crystallization (150°C, 48 h) (b) with and (a) without a ball milling.

milling produces a decrease in crystallite size and increase in the lattice strain of the faujasite phase rather than the silver iodide phase in the powder mixtures.

Crystalline formation during hydrothermal operation

The formation of several kinds of zeolitic phases was observed after the hydrothermal crystallization. X-ray diffraction results of hydrothermal operation with and without a ball milling is illustrated in Figure 6. The formed products, obtained in the autoclave containing the sodium hydroxide solution at 150°C, had a strong dependence on the increased milling time. In the absence of ball milling, the zeolite phases measured by XRD were not the iodide sodalite phase, but the hydroxyl-type phases; i.e., hydroxyl cancrinite, $Na_8Al_6Si_6O_{15}(OH)_6.4H_2O$, and analcime-O, $Na(Si_2Al)O_6.H_2O$, in which the iodine contents were detected only as strong peaks of silver iodide, γ-AgI. In this case, without ball milling, the I^- ions seem inaccessible to the fixation sites in the zeolite cages, and the iodine immobilization could not be confirmed.

On the other hand, with the ball milling operation, the phases detected by XRD were iodine sodalite, $Na_8(Al_6Si_6O_{24})I_2$, analcime-O, silver iodide and metallic silver, Ag. The iodine sodalite and analcime-O could be detected as sharp diffraction peaks with high intensities, even for the samples with the short milling time of 3 or 6 h, although the trace peaks of silver iodide remained in the pattern at the beginning of the ball milling. However, the milling operation lead to a decrease in the residual peaks of silver iodide with the increased milling time, and this caused formation of the Ag phase in the diffraction patterns, notably over 24 h. The overall route for the conversion process consists of two procedures; i.e., ball milling and hydrothermal conversion. Of the two procedures, the most critical in this study was the ball milling. With longer time, this enabled crystallization of the iodine sodalite at low temperature. Thus, the ball milling operation seems to contribute to the conversion of silver iodide to iodine sodalite.

Scanning electron micrographs of the powder obtained by ball milling at 700 rpm for 3, 6, 24, 48 h are shown in

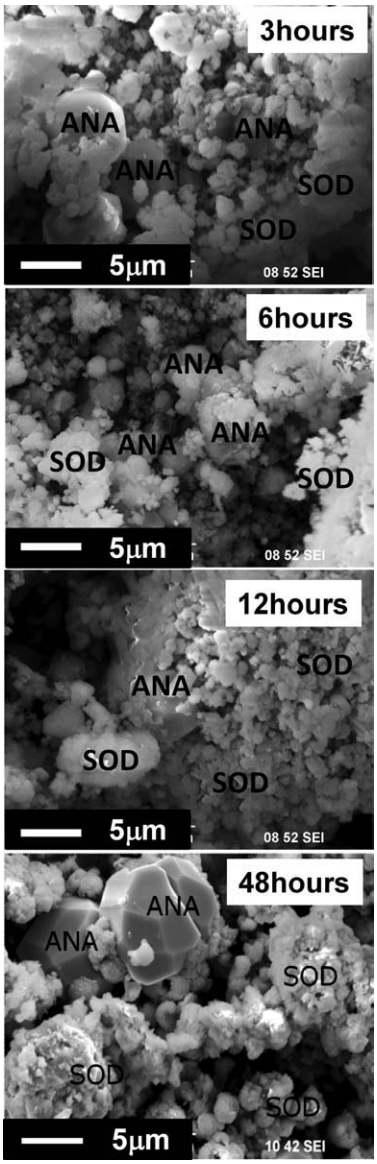

Figure 7. SEM photos of obtained powder after hydrothermal crystallization (150°C for 48 h) of milled sample (700 rpm for 3, 6, 12, 48 h).

ANA and SOD means analcime-O and sodalite, respectively.

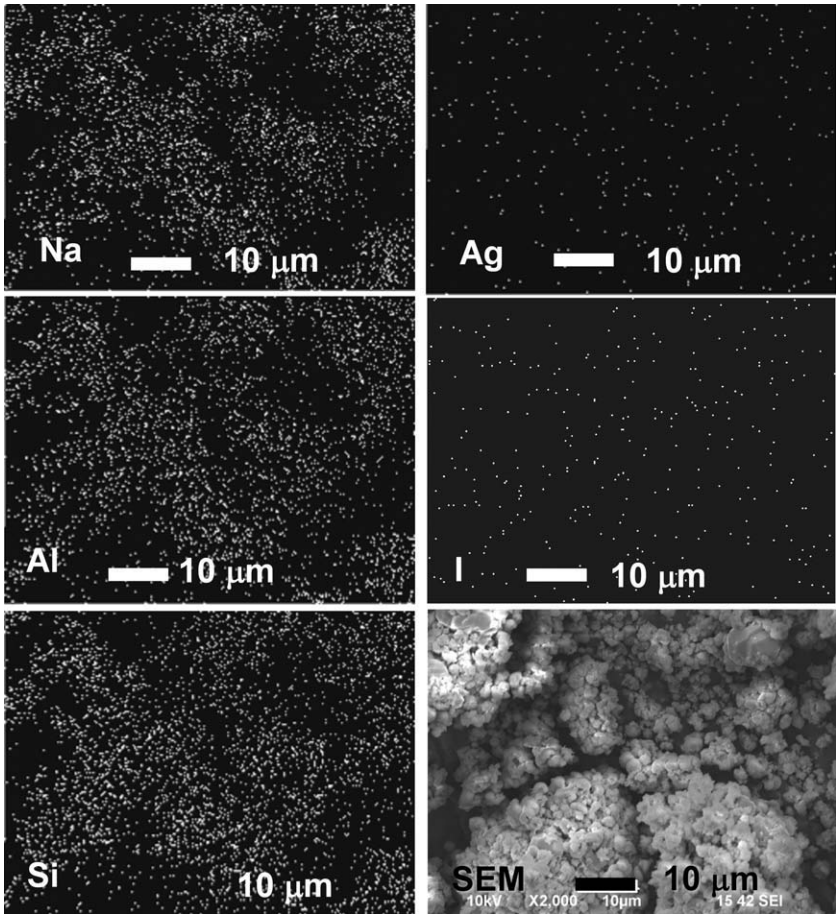

Figure 8. Elemental distribution (Na, Al, Si, Ag and I) of obtained powder after hydrothermal crystallization (150°C, 48 h) of milled sample (700 rpm 48 h).

Figure 7, and elemental distribution maps of the Na, Al, Si, Ag and I elements of the particles was displayed in Figure 8. As shown in Figure 7, the rhombic polyhedral particles, approximately 5–10 μm in diameter, were observed along with the agglomerates of small particles ($\sim$1 μm), although no apparent difference was observed in relation to the milling time. Although the polyhedral particle is the well-known typical shape of analcime well-crystallized under hydrothermal conditions,[19,20] the agglomeration of small particles was considered to be iodine sodalite. In fact, the energy dispersive spectroscopy analysis revealed that the Al/Si atomic ratio at spots on the agglomerate was 0.891 on average, whereas the value at another spot on the polyhedral particle was 0.440. The Al/Si atomic ratio on the agglomerate was as twice as that of the polyhedral particle. This approximately agreed with the deference in the Al/Si atomic ratio of the theoretical composition of each phase. In addition, the value of the Al/Si atomic ratio for analcime-O, ($Na(Si_2Al)O_6.H_2O$: Al/Si = 0.5), is equal to the original faujasite ($Na_2Al_2Si_4O_{12}.8H_2O$: Al/Si = 0.5), so that a part of the alumina silicate, which was in excess to the iodine total mass, seems to be easily composed of analcime-O as a byproduct of the hydrothermal reaction. The EDS analysis also revealed the homogeneous distribution of each element on the particles as shown in Figure 8, indicating that the agglomeration of the Ag and I elements was not present.

Figure 9 show the values of the lattice constant of sodalite calculated from several peaks; {1 1 0}, {2 1 1}, {2 2 2}, {3 3 3} at different milling times. The figure shows the average lattice constants for the obtained sodalites were a = 8.96–8.98. All the values were much larger than that of chlorine sodalite ($Na_8Al_6Si_6O_{24}Cl_2$, a = 8.88) which was estimated for natural sodalite, and were slightly smaller than the theoretical value of iodine sodalite ($Na_8Al_6Si_6O_{24}I_2$, a = 9.01).[16] This suggests that the iodine ion (I^-), which has a larger ion radius than that of hydroxyl ions (OH^-), was partially substituted for the original OH^- ions in the sodalite cages, which lead to the increasing lattice volume, a^3 of the sodalite crystals.

Iodine dissolution from the sodalite products

The leaching test results measured by ICP-MS are listed in Figure 10, which shows the effect of the milling time on the iodine leaching amount in ultrapure water and a sodium thiosulfate, $Na_2S_2O_3$, solution for 14 days. The ordinate shows the iodine concentration in mol dm^{-3} dissolved into the leachant, and the abscissa is the ball milling time. From this figure, it was found that the leaching amount of retained iodine was very low between 10^{-4} $\sim 10^{-5}$ in mol dm^{-3} when the original mixture was mechanically treated by ball mill, and the leaching amount slightly decreased when the milling time was longer. In ground water, thiosulfate can be formed as an intermediate compound in the reduction of sulfate. Silver iodide is more soluble in thiosulfate solution than in pure water. When the thiosulfate ion is present, the following complexation of silver enhances the silver iodide solubility

$$AgI + 2S_2O_3^{2-} \Leftrightarrow [Ag(S_2O_3)_2]^{3-} + I^-, \quad K = 3 \times 10^{-3} \quad (3)$$

This well explains the higher leaching amount value (1.01×10^{-2} mol dm^{-3}) without the ball milling operation (displayed as zero hour milling time) where silver iodide remained in the product as described earlier. Thus, it could be confirmed that the ball milling remarkably improved the stability of the product in the presence of thiosulfate under reducing conditions.

Conclusions

This study details a ball milling as a potential approach to convert and to immobilize radioactive iodine. As a result, iodine sodalite was successfully obtained by a combination of the ball milling and hydrothermal procedure from the mixture of silver iodide and zeolite 13X, the simulated spent adsorbents. The ball milling promoted the mechanochemical conversion from zeolite 13X and silver iodide crystals to form small crystal grains of faujasite and to enhance the lattice strain. The mechanical energy provided by ball milling produced a decrease in the crystallite size (~90 nm), and increase in lattice strain (~2.6%) of the faujasite phase rather than the silver iodide phase in the powder mixtures. During the crystallization of sodalite from the milled mixture, the formation of sodalite-type crystals with some impure phases, metallic silver, analcime-O and unreacted silver iodide, was confirmed as the results of the hydrothermal reaction at 150°C, 4.8 MPa. The unreacted silver iodide phase was confirmed to disappear in the product phase after the hydrothermal treatment when the ball milling was carried out over 24 h. SEM observations showed that the powder included two types of crystals which were characterized from their crystal shape as iodine sodalite and analcime-O. The lattice parameter of the obtained sodalite was nearly the theoretical value of iodine sodalite due to the expansion of the crystal lattice, although the values were slightly smaller than the theoretical value of iodine sodalite due to the partial substitution of iodine in the sodalite cages. Furthermore, the leaching amount from the milled sample was low on the order of 10^{-4} ~10^{-5} mol dm^{-3} regardless of the leachant. This conversion route has practical potential for the low-temperature processing of a spent adsorbent and possibly the safety process without re-emission of radioactive iodine.

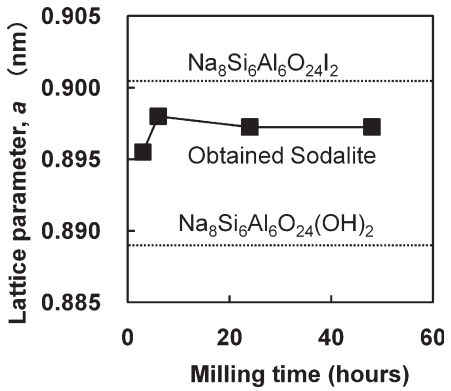

Figure 9. Effect of milling time on lattice parameter, *a* of sodalite crystal obtained after hydrothermal crystallization (150°C, 48 h).

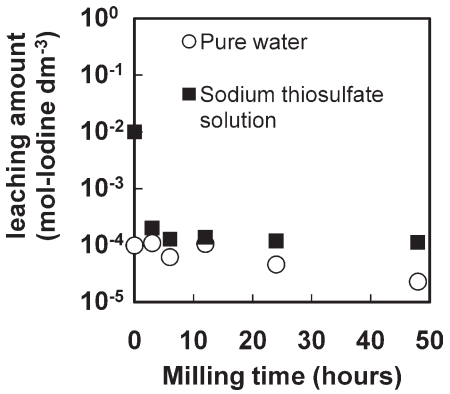

Figure 10. Effect of milling time on iodine leaching in pure water (circles) and $Na_2S_2O_3$ solution (squares) as matrices.

The leachability test was carried out for 14 days at room-temperature.

Acknowledgments

This work was supported by JSPS, KAKENHI "Grant-in-Aid for Exploratory Research" (Grant No. 23656588).

Literature Cited

1. Burger LL, Scheele RD, Halko BT. Comparison of silver sorbents for application to radioiodine control at the purex process facility modification. [Iodine 129]. *US DOE Report*. 1988;PNL–6607/UC-510.
2. Burger LL, Scheele RD, Matsuzaki CL. Methyl iodine sorption by reduced silver mordenite. *US DOE Report*. 1983; PNL-4498/UC-70.
3. Rovnyi SI, Pyatia NP, Istomin IA. Catching of 129I during processing of spent fuel from power plants. *Atomic Energy*. 2002;92: 534–535.
4. Taylor P, Lopata VJ, Wood DD, Yacyshyn H. Environmental aspects of stabilization and solidification of hazardous and radioactive wastes. *ASTM STP*. 1989;1033:287–301.
5. Atkins M, Glasser FP. Application of Portland cement-based materials to radioactive waste immobilization. *Waste Manage*. 1992;12: 105–131.
6. Noshita K, Nishi T, Yoshida T, Fujihara H, Marase T. Vitrification technique of radioactive waste using AgI-Ag_2O-P_2O_5 glass system. *Paper presented at: the Radioactive Waste Management and Environmental Remediation*; 1999:107–112; New York, NY.
7. Garino TJ, Nenoff TM, Krumhansl JL, Rademacher DX. Low-temperature sintering Bi-Si-Zn-oxide glasses for use in either glass composite materials or core/shell 129I waste forms. *J Am Ceram Soc*. 2011:94. doi:10.1111/j.1551–2916.2011.04542.x. In press.
8. Watanabe Y, Ikoma T, Yamada H, Suetsugu Y, Komatsu Y, Stevens GW, Moriyoshi Y, Tanaka J. Novel long-term immobilization method for radioactive iodine-129 using a zeolite/apatite composite sintered body. *Appl Mater Interfaces*. 2009;1:1579–1584.
9. Babad H, Strachen DM. Method for immobilizing radioactive iodine. US patent 4, 229,317. 1980.
10. Trevorrow LE, Vandegrift GF, Kolba VM, Steindler MJ. Compatibility of technologies with regulations in the waste management of H-3, I-129, C-14, and Kr-85: Part I. Initial information base. *US DOE Report*. 1983;ANL-83–57-Pt.1.
11. Trevorrow LE, Kolba VM, Vandegrift GF, Steindler MJ. Compatibility of technologies with regulations in the waste management of H-3, I-129, C-14, and Kr-85: Part II. Analysis. *US DOE Report*. 1983;ANL-83–57-Pt.2.
12. Buhl JC. The properties of salt-filled sodalite. Part 4. Synthesis and Heterogeneous Reactions of Iodate-Enclathrated Sodalite $Na_8[AlSiO_4]_6(IO_3)_{2-x}(OH.H_2O)_x$; $0.7<x<1.3$. *Thermochimica Acta*. 1996; 286:251–262.

13. Babad H, Strachen DM. Iodide and iodate sodalites for the long-term storage of iodine-129. *US DOE Report*. 1979; RHO-SA-83. Paper presented at: American Ceramics Society International Symposium on Ceramics in Nuclear Waste Management; 1979; Columbus, OH.
14. Richardson JW Jr. Salt-occluded zeolite waste forms: Crystal structures and transformability. *US DOE Report*. 1996; ANL/RE/CP-93201. Paper presented at: Material Research Society Symposium; 1996; CONF-961202.
15. Hyatt NC, Hriljac JA, Choudhry A, Malpass L, Sheppard G, Maddrell ER. Zeolite-salt occlusion potential route for the immobilisation of iodine-129? *Mater Res Soc Proc*. 2004;807: 359–364.
16. Bardez I, Campayo L, Rigaud D, Chartier M, Calvet A. Study of the sodalite phase for the conditioning of halide salts (NaCl and NaI): Comparison of two synthesis routes: Presented at: Atlante 2008; 2008;O4–19; Montpellier, France.
17. Bates SO, Pieple GF, Johnston JW. Leach testing of simulated hanford waste vitrification plant reference glass HW-39. *US DOE Report*. 1989:PNL-6884-Pt.1.
18. Jenkins R.Snyder RO. *Introduction to X-ray Powder Diffractometry*. Chichester, UK: John Wiley & Sons, Inc., 1996;89–91.
19. Liou JG. Analcime equilibria. *Lithos*. 1971;4:389–402.
20. Pechar F. Hydrothermal analcime synthesis at 10 MPa isobar. *Cryst Res Technol*. 1989;24:871–877.

Manuscript received June 2, 2011, and revision received Aug. 8, 2011.